Vol 15 No 4, April 2006
1009-1963/2006/15(04)/0778-14

Chinese Physics

© 2006 Chin. Phys. Soc.
and IOP Publishing Ltd

Numerical simulation of dendrite growth and microsegregation formation of binary alloys during solidification process*

Li Qiang(李 强)[a)†], Guo Qiao-Yi(郭巧懿)[b)], and Li Rong-De(李荣德)[a)]

[a)] *School of Material Science and Engineering, Shenyang University of Technology, Shenyang 110023, China*

[b)] *Shenyang Ligong University, Shenyang 110168, China*

(Received 8 November 2005; revised manuscript received 28 December 2005)

The dendrite growth and solute microsegregation of Fe-C binary alloy are simulated during solidification process by using cellular automaton method. In the model the solid fraction is deduced from the relationship among the temperature, solute concentration and curvature of the solid/liquid interface unit, which can be expressed as a quadric equation, instead of assuming the interface position and calculating the solid fraction from the interface velocity. Then by using this model a dendrite with 0 and 45 degree of preferential growth direction are simulated respectively. Furthermore, a solidification microstructure and solute microsegregation are simulated by this method. Finally, different Gibbs-Thomson coefficient and liquid solute diffusing coefficient are adopted to investigate their influences on the morphology of dendrite.

Keywords: dendrite, simulation, cellular automaton, solidification
PACC: 6150C, 6185, 8130

1. Introduction

Dendrite is a classic morphology of crystal during solidification process. Studying the dendrite evolution is helpful to better understanding the essence of solidification microstructure and solutal microsegregation. In the past decades lots of researchers used different methods to study the dendrite evolution. Amar, Brener *et al* used the theoretical method to describe the dendrite formation.[1−4] Spittle and Brown used the Monte Carlo method to simulate the morphology of solidification microstructure.[5] Gandin and Rappaz adopted the cellular automaton (CA) method to simulate solidification microstructure.[6] Karma and Rappel applied the Phase field method to simulate the dendrite evolution.[7] Juric and Tryggvason used the Front-Tracking method to simulate dendrite evolution.[8] Kim *et al* used Level-set method to simulated the dendrite evolution.[9] At present, phase field method and CA method are the two major methods in numerical simulation of the dendrite evolution, and lots of researchers prefer to adopt the phase field method to simulate dendritic morphology.[10,11] However, the phase field method is limited by the meshed grid size. Compared with other methods, CA method has such advantages that it has simple rules, no restriction by meshed grid size and no need to track the topology of the solid/liquid interface.

Former researchers[6,12,13] who used CA method to simulate solidification microstructure only considered the thermal diffusion without considering the solute diffusion effects. In 1997 Dilthy *et al*[12] presented a CA model for both thermal and solutal dendrite based on the thermal and solutal diffusion mechanism. In 1999 Nastac[15] presented a model combined the thermal diffusion and solutal diffusion together, and the model can simulate the columnar-to-equiaxal transition and show the interaction among the growth dendrites. Jocat *et al*[16] presented a pseudo-front tracking method that is similar to CA method, in which the solid fraction of the solid/liquid interface unit is got by Thermal-Cal software. However, the model is based on the assumption of uniform temperature in the whole simulated zone. Sanchez and Stefanescu[17]

*Project supported by the Educational Department of Liaoning Province (Grant No 05L304).
†E-mail: lq5393@sina.com.cn

modified the method of calculating the solid/liquid interface curvature in a local meaning to replace the method of counting the solid fraction of the nearest neighbour cell adopted by Dilthy, *et al.*[12−15]

All these works of the CA method mentioned above assumed that there was a sharp-interface and the interface position was known so that the solid fraction in the interface can be found according to the interface position and interface velocity. However, the shape and position of dendrite morphology is not defined, it leads to the inaccurate solution of the solid fraction in the solid/liquid interface unit. In order to overcome this weakness, Jacot and Rappaz combined the Thermal-Calc software with CA model to calculate the solid fraction in multicomponent alloys solidification.[16] However, those without the software cannot use this method. But the method Jacot used presents an idea that the solid fraction of the solid/liquid interface unit can be obtained by calculating via the phase diagram method. Therefore, in this paper an improved model is presented to calculate the solid fraction of the solid/liquid interface unit according to the equilibrium phase diagram, in which the exact position of the interface position need not to be known and the solid fraction of the interface unit can be obtained by solving a quadric equation. The essence of the model is that if the solute concentration, temperature and the curvature of a random unit are known, and all these state parameters responding to a point in the phase diagram can be deduced. Therefore, if the state parameters are known, the solid fraction can be got according the phase diagram. In order to illustrate the main idea of the model, Fe-0.6%C binary alloy is adopted in this paper.

2. Mathematical physical model

This model is based on the following assumptions: 1) the density of the alloy is assumed as a constant, which is not changed during solidification process; 2) there exists a local phase equilibrium state in the solid–liquid mushy zone; 3) the influences of liquid convection are ignored; 4) there are three kinds of phase states, solid, liquid and the solid/liquid interface that the solid fraction ranges from zero to one, in addition, the solid/liquid interface unit must lie between the solid and liquid units.

The energy conservation equation is

$$\frac{\partial T}{\partial t} = \nabla \cdot (\alpha \nabla T) + Q, \tag{1}$$

where T is temperature, t is time, α is the thermal diffusion coefficient, and $\alpha = \dfrac{k}{\rho C_{\mathrm{p}}}$, k is the conductivity, ρ is density, C_{p} is the specific heat, Q is the latent heat released as the solid/liquid interface advances into the undercooled liquid:

$$Q = \frac{\partial f_{\mathrm{s}}}{\partial t} \frac{L_{\mathrm{h}}}{C_{\mathrm{p}}}, \tag{2}$$

where f_{s} is the solid fraction of the solid/liquid interface zone, L_{h} is the latent heat per unit volume. The solute diffusion governing equation is

$$\frac{\partial C_I}{\partial t} = \nabla \cdot (D_I \nabla C), \tag{3}$$

where D is the solute diffusion coefficient, the subscript I stands for the liquid or solid. When the interface advances, solute will be redistributed in the solid/liquid interface unit, there is a relation

$$C_{\mathrm{s}}^* = k_{\mathrm{p}} C_{\mathrm{l}}^*, \tag{4}$$

where k_{p} is the solute partition coefficient, which is assumed as a constant, C_{l}^* is the liquid solute concentration in the liquid side of the solid/liquid interface unit, C_{s}^* is the solid solute concentration in the solid side of the solid/liquid interface unit.

According to the phase diagram, if the kinetic undercooling is neglected, the relationship among the solute concentration, curvature and temperature in the solid/liquid interface unit can be expressed as

$$T^* = T_{\mathrm{eq}} + m(C_{\mathrm{l}}^* - C_0) + \Gamma K f(\theta, \varphi), \tag{5}$$

where m is liquidus slope, which is a constant, Γ is the Gibbs-Thomson coefficient, K is the curvature of the solid/liquid interface, $f(\theta, \varphi)$ is the anisotropic function, which can be got according to Ref.[17], θ is the normal direction of the solid/liquid interface, φ is the preferential growth direction. The curvature of the solid/liquid interface can be deduced from the formula of curvature definition:[17−19]

$$K = \frac{z''}{(1 + z'^2)^{3/2}}, \tag{6}$$

where z' and z'' are the first and second derivatives of the solid fraction respectively, they are

$$z' = \frac{\mathrm{d}y}{\mathrm{d}x} = \frac{\mathrm{d}f_\mathrm{s}/\mathrm{d}x}{\mathrm{d}f_\mathrm{s}/\mathrm{d}y} = \frac{(f_\mathrm{s})_x}{(f_\mathrm{s})_y}, \tag{7}$$

$$z'' = \frac{\mathrm{d}(y')}{\mathrm{d}x} = \frac{\mathrm{d}f_\mathrm{s}/\mathrm{d}x}{\mathrm{d}f_\mathrm{s}/(\mathrm{d}y')} = \frac{(f_\mathrm{s})_x^2(f_\mathrm{s})_{yy} + (f_\mathrm{s})_y^2(f_\mathrm{s})_{xx} - 2(f_\mathrm{s})_x(f_\mathrm{s})_y(f_\mathrm{s})_{xy}}{(f_\mathrm{s})_y^3}. \tag{8}$$

From Eqs.(6)–(8), we have

$$K = \frac{z''}{(1+z'^2)^{3/2}} = \frac{2(f_\mathrm{s})_x(f_\mathrm{s})_y(f_\mathrm{s})_{xy} - (f_\mathrm{s})_x^2(f_\mathrm{s})_{yy} - (f_\mathrm{s})_y^2(f_\mathrm{s})_{xx}}{((fs)_x^2 + (fs)_y^2)^{3/2}} \tag{9}$$

the subscripts x and y represent the deviations of the solid fraction in x and y-axis direction respectively.

Equation (1) can be divided into two parts. In the first part, the latent heat is neglected and the heat diffusion is considered only, which can be expressed as Eq.(10), in the second part the heat diffusion is neglected and latent heat is considered only, which can be expressed as

$$\frac{\partial T}{\partial t} = \alpha\nabla^2 T, \tag{10}$$

$$T' = T + \frac{L_\mathrm{h}}{c_\mathrm{p}}\frac{\partial f_\mathrm{s}}{\partial t}, \tag{11}$$

where T' is the temperature which considered that the latent heat is released. Therefore, Eq.(11) can be rewritten as

$$T' = T + \frac{L_\mathrm{h}}{c_\mathrm{p}}(f_\mathrm{s}^{n+1} - f_\mathrm{s}^n), \tag{12}$$

where $n+1$ and n stand for the $(n+1)$th and the nth steps respectively.

In this article there are three kinds of solute concentration, which are liquid solute concentration, solid solute concentration and average solute concentration respectively. In the solid phase, the average solute concentration is equal to the solid solute concentration and the liquid solute concentration is equal to zero. In the liquid phase the average solute concentration is equal to the liquid solute concentration and the solid solute concentration is equal to zero. In the solid/liquid interface unit, the average solute concentration is equal to the sum of the solid fraction multiplying the solid solute concentration and the liquid fraction multiplying the liquid solute concentration. Therefore the average solute concentration is expressed as

$$\overline{C} = \begin{cases} C_\mathrm{l}, & f_\mathrm{s} = 0, \\ C_\mathrm{s}^* f_\mathrm{s} + C_\mathrm{l}^*(1-f_\mathrm{s}), & 0 < f_\mathrm{s} < 1, \\ C_\mathrm{s}, & f_\mathrm{s} = 1, \end{cases} \tag{13}$$

where $\overline{C}$ is average solute concentration, the subscripts l and s correspond to liquid and solid phase respectively.

According to Eq.(13), it can be deduced that the liquid solute concentration in the solid/liquid unit is given as

$$\begin{aligned} C_\mathrm{l}^* =& \frac{\overline{C}}{(1 - f_\mathrm{s}^{n+1} + k_\mathrm{p}\cdot f_\mathrm{s}^{n+1})} \\ =& \frac{\overline{C}}{(1-(1-k_\mathrm{p})\cdot f_\mathrm{s}^{n+1})}. \end{aligned} \tag{14}$$

Combining the Eq.(5) with Eq.(11), we can get

$$\begin{aligned} T' =& T^* = T + \frac{L}{C_\mathrm{p}}(f_\mathrm{s}^{n+1} - f_\mathrm{s}^n) \\ =& T_\mathrm{eq} + m(C_\mathrm{l}^* - C_0) - \Gamma K f(\theta,\varphi). \end{aligned} \tag{15}$$

Substituting Eq.(14) into Eq.(15), we have

$$\begin{aligned} & T + \frac{L}{C_\mathrm{p}}(f_\mathrm{s}^{n+1} - f_\mathrm{s}^n) \\ =& T_\mathrm{eq} + m\left(\frac{\overline{C}}{1-(1-k_\mathrm{p})\cdot f_\mathrm{s}^{n+1}} - C_0\right) \\ & - \Gamma K f(\theta,\varphi). \end{aligned} \tag{16}$$

Eq.(16) can be rewritten as

$$\begin{aligned} & \left(T_\mathrm{eq} - T + \frac{L}{C_\mathrm{p}}f_\mathrm{s}^n - mC_0 - \Gamma K f(\theta,\varphi)\right) \\ & \cdot (1-(1-k_\mathrm{p})\cdot f_\mathrm{s}^{n+1}) \\ & - \frac{L}{C_\mathrm{p}}f_\mathrm{s}^{n+1}\cdot(1-(1-k_\mathrm{p})\cdot f_\mathrm{s}^{n+1}) + m\overline{C} = 0. \end{aligned} \tag{17}$$

Eq.(17) can be simplified as

$$A\cdot(f_\mathrm{s}^{n+1})^2 + B\cdot f_\mathrm{s}^{n+1} + C = 0, \tag{18}$$

where A, B and C are coefficients, which can be expressed as

$$\begin{aligned} A =& \frac{L}{C_{\mathrm{p}}}(1-k_{\mathrm{p}}), \\ B =& -\left(T_{\mathrm{eq}}-T+\frac{L}{C_{\mathrm{p}}}\cdot f_{\mathrm{s}}^{n}-mC_0-\Gamma K f(\theta,\varphi)\right) \\ & \cdot(1-k_{\mathrm{p}})-\frac{L}{C_{\mathrm{p}}}, \\ C =& T_{\mathrm{eq}}-T+\frac{L}{C_{\mathrm{p}}} \\ & \cdot f_{\mathrm{s}}^{n}-mC_0-\Gamma K f(\theta,\varphi)+m\overline{C}. \end{aligned} \tag{19}$$

Equation (18) is a classic quadric equation, which have two roots at most. If $B^2-4AC>0$, Eq.(18) has two roots, which can be given as

$$f_{\mathrm{s}1,2}=\frac{-B\pm\sqrt{B^2-4AC}}{2A}. \tag{20}$$

If the Eq.(17) has two roots, the two roots of the equation must be beside $-\dfrac{B}{2A}$, one is bigger than $-\dfrac{B}{2A}$, and the other is smaller than $-\dfrac{B}{2A}$.

It is easy to show that for the two roots of Eq.(18), there are only one $f_{\mathrm{s}}^{n+1}\in[f_{\mathrm{s}}^{n},1]$ if $T_{\mathrm{a}}\le T\le T_{\mathrm{c}}$, and $f_{\mathrm{s}}^{n+1}\in[0,f_{\mathrm{s}}^{n}]$ if $T_{\mathrm{c}}\le T\le T_b$, where

$$\begin{aligned} T_a &= T_{\mathrm{s}}(\overline{C})-\frac{L}{C_{\mathrm{p}}}(1-f_{\mathrm{s}}), \\ T_b &= T_{\mathrm{l}}(\overline{C})+\frac{L}{C_{\mathrm{p}}}f_{\mathrm{s}}, \\ T_c &= T_{\mathrm{eq}}-mC_0+\frac{m\cdot\overline{C}}{1-(1-k_{\mathrm{p}})\cdot f_{\mathrm{s}}^{n}}, \\ T_{\mathrm{s}}(\overline{C}) &= T_{\mathrm{eq}}+m(\frac{\overline{C}}{k_{\mathrm{p}}}-C_0), \\ T_{\mathrm{l}}(\overline{C}) &= T_{\mathrm{eq}}+m(\overline{C}-C_0), \end{aligned} \tag{21}$$

where $T_{\mathrm{l}}(\overline{C})$ and $T_{\mathrm{s}}(\overline{C})$ are the liquidus and solidus temperature at the solute concentration $\overline{C}$, C_0 is the initial solute concentration, C_0=0.6.

The boundary condition and initial conditions are

$$\begin{aligned} &\frac{\partial T}{\partial t}=h(T-T_{\mathrm{sur}}), \\ &T(x,y,t=0)=T_0, \\ &C(x,y,t=0)=C_0, \end{aligned} \tag{22}$$

where h is the interface heat transferring coefficient on the boundary, T_{sur} is the surrounding temperature, which is assumed to be a constant, T_0=25°C, T_0 is initial temperature.

The advancing velocity of the solid/liquid interface can be given as

$$V=\left[D_{\mathrm{s}}\left(\frac{\partial C_{\mathrm{s}}}{\partial n}\right)_{\mathrm{s}}-D_{\mathrm{l}}\left(\frac{\partial C_{\mathrm{l}}}{\partial n}\right)_{\mathrm{l}}\right]/(C^{*}(1-k_{\mathrm{p}})). \tag{23}$$

Time step is an important factor affecting the calculating efficiency, which can be calculated according to the following equation:

$$\delta t\le\frac{1}{5}\min\left(\frac{a^2}{D_{\mathrm{l}}},\frac{a^2}{D_{\mathrm{s}}},\frac{a^2}{\alpha},\frac{a}{V_{\max}}\right), \tag{24}$$

where min is an operation of selecting the minimum value among $\dfrac{a^2}{D_{\mathrm{l}}}$, $\dfrac{a^2}{D_{\mathrm{s}}}$, $\dfrac{a^2}{\alpha}$ and $\dfrac{a}{V_{\max}}$, δt is time step, $V_{\max}$ is the maximum velocity in the all solid/liquid interface unit, a is the size of the meshed grid, 1/5 means that the advancing interface can't move over 1/5 of meshed grid in each time step. In other words, the solid fraction can also be checked according to Eq.(24), the reasonable solution of solid fraction should satisfy $|f_{\mathrm{s}}^{n+1}-f_{\mathrm{s}}^{n}|\le 0.2$.

The CA rules of nucleation and capturing are adopted as in Ref.[15,17]. The calculation steps is given as follows:

1) setting the initial and boundary conditions according to Eq.(22);

2) calculating the time step according to Eq.(24);

3) calculating the temperature field without considering the latent heat releasing according to Eq.(10);

4) calculating the solid fraction in the solid/liquid interface unit according to Eq.(18);

5) bringing the new solid fraction of the solid/liquid interface unit into Eqs.(6), (12) and (14) to get the curvature, interface temperature and solute concentration of the solid/liquid interface unit;

6) the solute concentration based on Eq.(3) that takes the change of the solute concentration in the solid/liquid interface unit into account;

7) Restoring the variable data, such as temperature, solute concentration, curvature and solid fraction;

8) repeating the above steps until reaching the appointed calculating number.

In this paper Fe-0.6%C binary alloy was adopted, and the parameters used in this paper are listed in Table 1. The size of meshed grid is 1μm×1μm, and the whole simulated zone is 0.25mm×0.25mm.

Table 1. The parameters used in the model.[13]

Density/(kg/m^3)	7300
Heat diffusion coefficient/(m^2/s)	6.1×10^{-6}
Solute diffusion coefficient in liquid phase/(m^2/s)	2×10^{-9}
Solute diffusion coefficient in solid phase/(m^2/s)	5×10^{10}
Latent heat/(kJ/kg)	270
Specific heat/(J/kg·K)	800
Liquidus slope in equilibrium condition	–80
Gibbs–Thomson coefficient/(m·K)	1.9×10^{-7}
Partition coefficient in equilibrium condition	0.34
Melting temperature/°C	1490
Initial temperature/°C	1480
Boundary heat transfer heat coefficient/(W/m·K)	1000

In order to simplify the simulation, firstly, a solid seed is put into the center of the simulated zone, whose preferred growth directions are 0 and 45 degree. And then a solidification microstructure is simulated in the same solidification conditions. Finally, the different Gibbs–Thomson coefficients and liquid solute diffusing coefficients are adopted to study their effects on morphology of the dendrite and microsegregation.

3. Results and analysis

Figure 1 indicates that a solid seed grows as the solidification time increases. The grey-scale bar in the right side of Fig.1 corresponds to the different solute

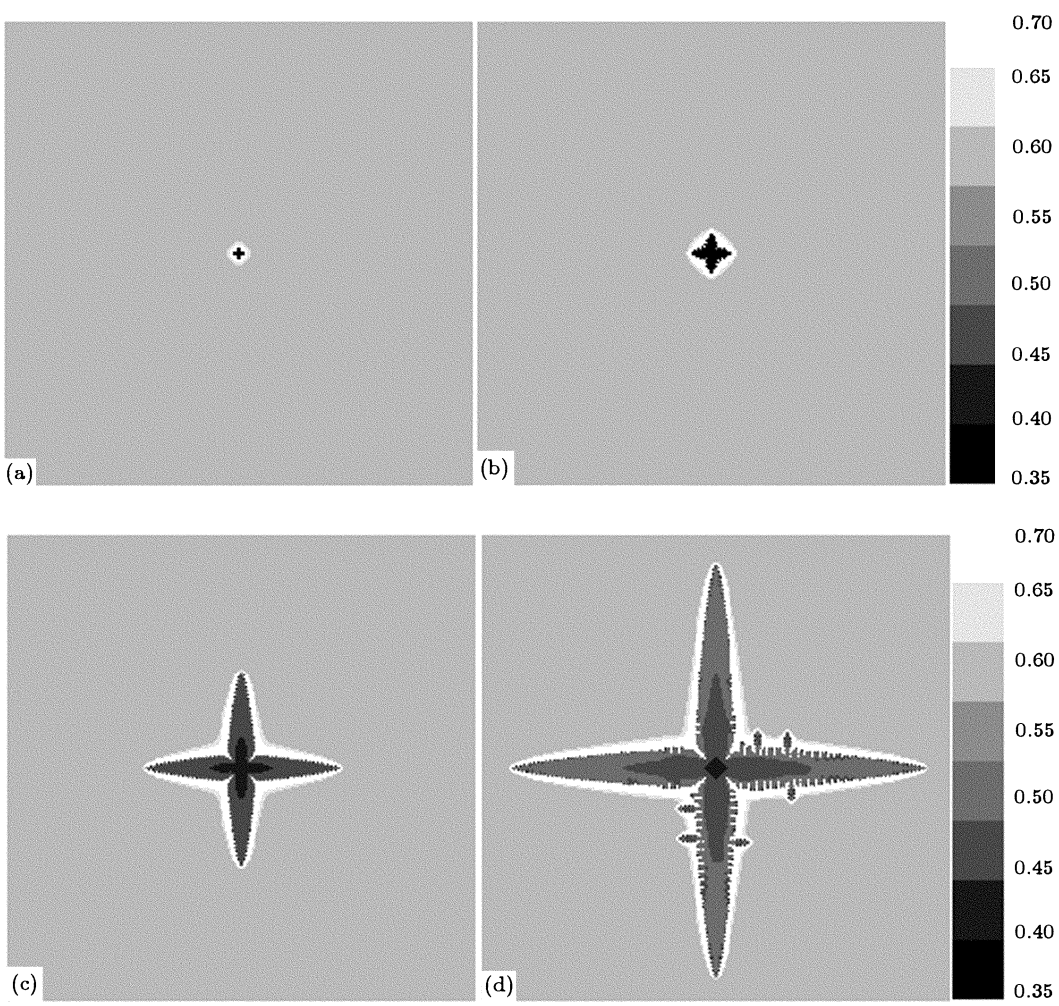


Fig.1. The dendrite morphology at different solidification time, whose preferential growth direction is 0 corresponded to the horizontal direction. t=0.002, 0.006, 0.012, 0.016s, respectively.

concentration. When the solidification time is 0.002s, the solid seed prefers to grow along the vertical and horizontal direction, which can be seen in Fig.1(a). When the solidification time is 0.06s, the solid seed becomes a dendrite, as shown in Fig.1(b). In the Fig.1(c),(d), it is shown that the dendrite grows up, and the solute concentration in the primary dendritic arm also rises gradually because of the solute back-diffusion in the solid phase. When the solidification time is 0.016s, the second dendrite arms appear at the roots of the primary dendritic arm because the undercooling caused by the solute concentration is much bigger than the undercooling caused by the temperature. In addition, Fig.1 shows that the solute concentration in primary dendrite arms rises up as the solidification time increases due to the solute back diffusion. The solute concentration of the concave part of the dendrite contour is higher than that in the protruding part of the dendrite contour. Finally, the simulated dendrite morphology is similar to the results shown in Ref.[17].

In order to investigate whether the dendritic growth satisfied the Ivanstov parabolic growth law or not, the relationship between the position and growth velocity of the dendritic tip and the solidification time is drawn in Fig.2.

Figure 2(a) shows that the relationship between the dendrite tip position and solidification time approaches to the parabolic distribution, which indicates that the solid seed is satisfied with Ivanstov's parabolic growth law. Figure 2(b) shows that the growth velocity of the dendrite tip increases as the solidification time increases at beginning of solidification. However, when the solidification time is out of 0.01s, the growth velocity of dendritic tip will not rise any more. At the beginning of solidification, the difference of the solute concentration gradient beside the dendritic tip is much small, as the solidification time increases, the difference of the solute concentration gradient beside the solid/liquid interface increases, which leads to the gradual increase of the growth velocity of dendritic tip. When the solidification time is more than 0.01s, the difference of the solutal gradient keep constant approximately and the growth velocity does not rise any more.

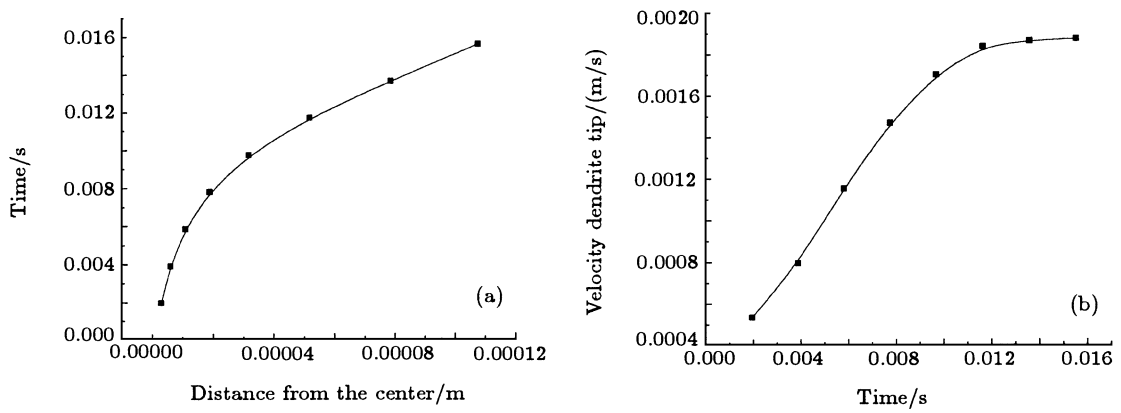


Fig.2. The advancing distance and velocity of the solid/liquid interface at different solidification time.

Figure 3 shows the solid fraction and temperature evolution of the solid/liquid interface unit. Figure 3(a) indicates that the solid fraction increases rapidly at the beginning of solidification. As the solidification continues, the solid fraction of the solid/liquid interface unit increases steadily and the dendrite growth velocity is approximately the same in this period until the solid fraction reaches one. Fig.3(b) shows the temperature evolution of the solid/liquid interface unit. At the beginning of solidification the temperature drops down quickly. As t=9.7×10^{-6}s, f_s=0.25, the temperature of solid/liquid interface unit, T=1481.04°C, is higher than the initial temperature because the latent heat released by the solid/liquid interface advancing can't diffuse to the outside immediately so that temperature of the solid/liquid interface unit rises and becomes higher than initial temperature. As the solidification continues, more and more heat is transferred to the outside, which leads to the decrease of the temperature of the solid/liquid interface unit.

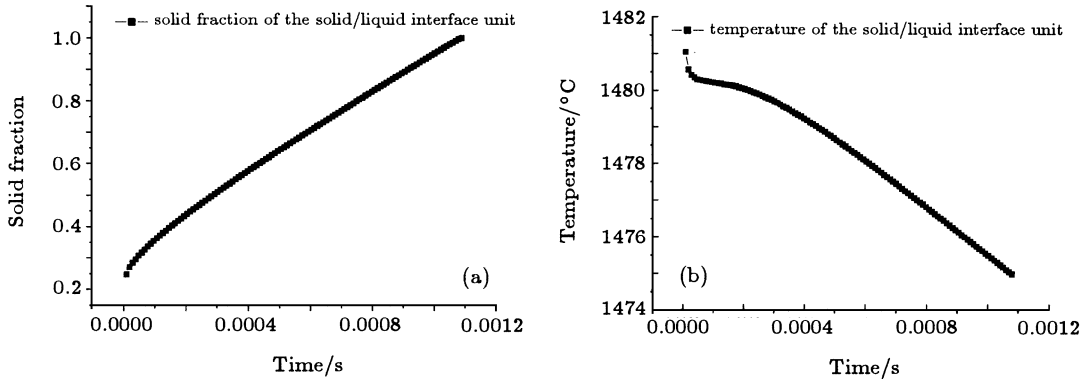


Fig.3. Solid fraction and temperature of the solid/liquid interface unit.

Figure 4 shows the temperature distribution along the centreline during solidification process. In Fig.4(a), the highest temperature is about 1479.25°C at t=0.0004s, and the lowest temperature is about 1476.5 °C on the boundary. The difference between the highest and lowest temperature is near 3°C. As t=0.0039s, in Fig.4(b), the highest temperature is about 1457.25°C and the lowest temperature is about 1453.5°C, the difference between the highest temperature and the lowest temperature is near 4°C. Figure 4 shows that the highest temperature along the centreline is in the middle of the centreline because the heat is generated in the inner side of liquid and the heat is extracted to the outside through the boundary. Figure 4 indicates that the temperature difference along the centreline will increase as the solidification time increases.

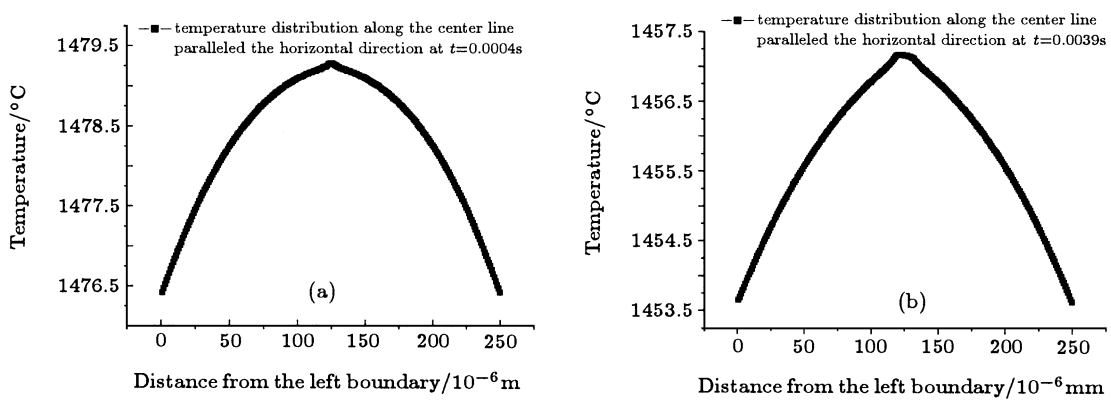


Fig.4. Temperature distribution in the centreline at t=0.0004 and 0.0039s respectively.

Figure 5 is the solute concentration distribution that can also display the dendrite morphology, in which the preferential growth direction is 45 degree with horizontal direction. As the solidification time is 0.006s, the solid seed grows up. When the solidification time is 0.012s, the second dendrite arms appear in the primary dendrite arms. When the solidification time is 0.023s, more and more second dendrite arm appears, and the solute concentration in the second dendrite arms is higher than that in the primary dendrite arms. Compared Fig.5 with Fig.1, it is easily found that the second dendrite arms rise more easily because the thermal undercooling in Fig.5 is much smaller due to its preferential growth direction.

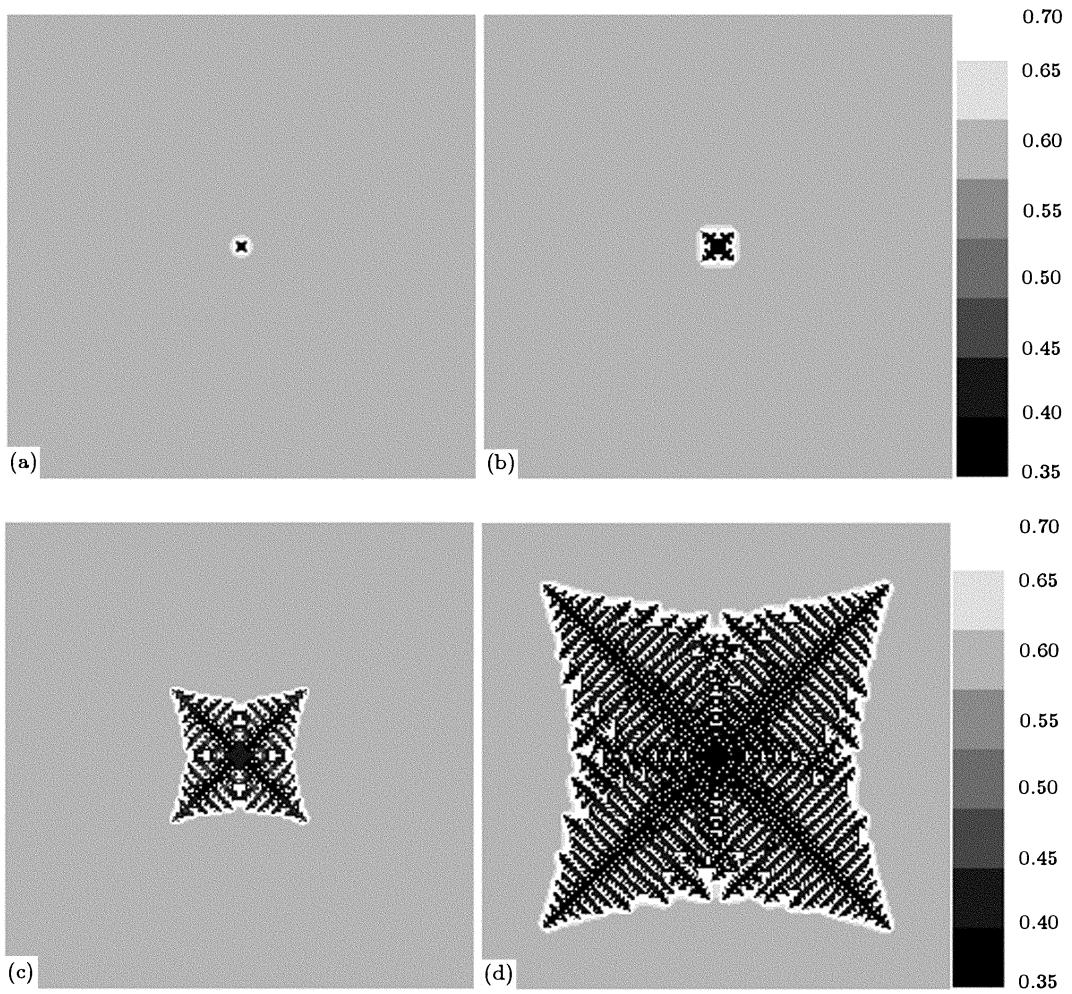


Fig.5. Dendrite morphology at different solidification time: t=0.002s, 0.006s, 0.012s and 0.023s respectively.

Figure 6 is the dendrite morphology at different solidification time, and the grey-scale bar in the right side of the figure corresponds to the solute concentration. When the solidification time is 0.002s, some nuclei forms randomly in the undercooling liquid, as shown in Fig.6(a). When the solidification time is 0.008s, in Fig.6(b), some nuclei are preferred to grow along the horizontal direction, the others are preferred to grow in 45 degree about the horizontal direction. As the solidification time is 0.019s, in Fig.6(d), some dendrite will grow continuously until they meet one each other or reach the boundary. When the two dendrites meet, there will be a rich solute zone between the two primary dendrite arms, which leads to solute microsegregation after solidification.

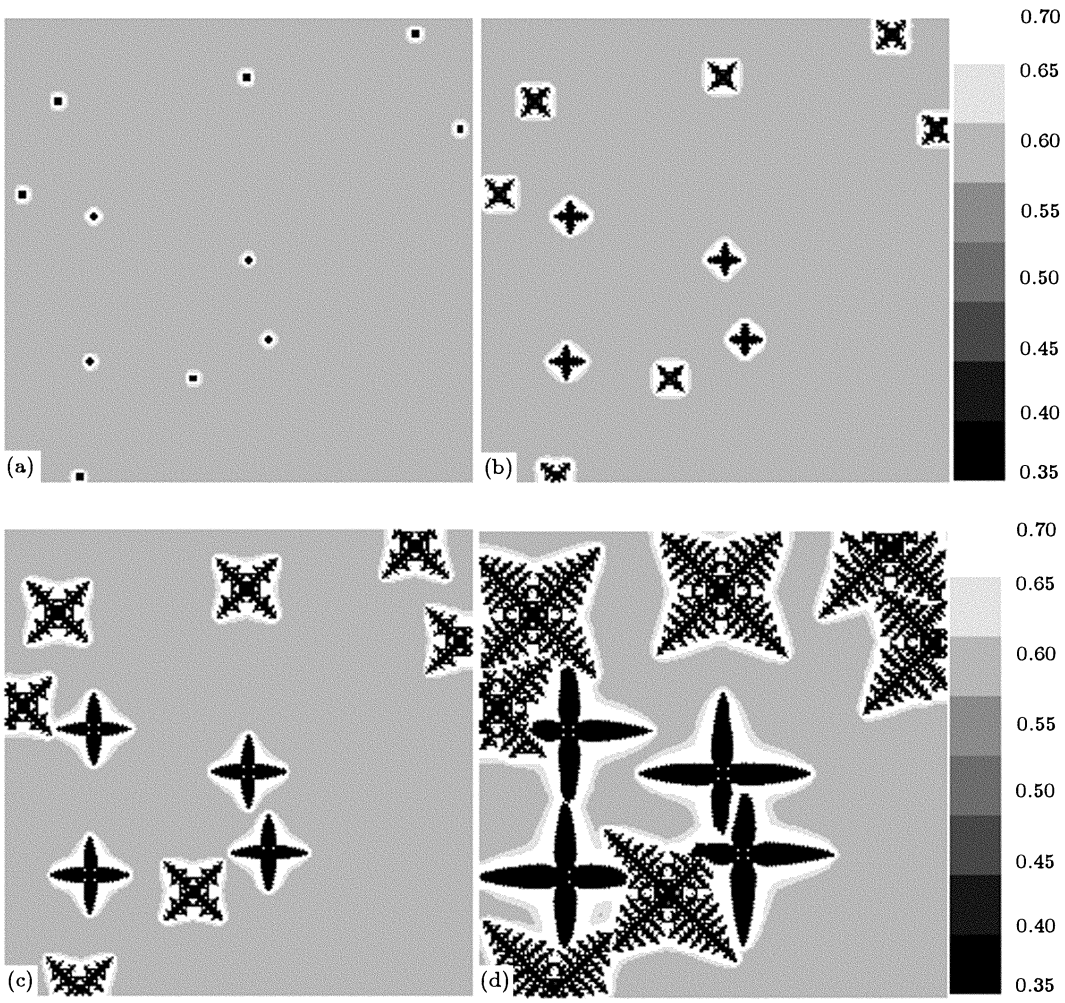


Fig.6. Microstructure at different solidification times t=0.002, 0.008, 0.01 and 0.019s respectively.

Figure 7 shows the dendrite morphology, the grey-scale bar in the right side indicates the solute concentration. As the Gibbs–Thomson coefficient decreases as one tenth of the normal value, there is not much change of the dendrite morphology. In addition, in Fig.7(a) the solid seed begins to grow with preferential growth direction along the horizontal and vertical direction, and the solute concentration of the solid seed is about 0.4%. When solidification time is 0.008s, the solute concentration in the solid seed rise up to 0.5 for the solute back diffusing. As the solidification time is 0.016s, the solute concentration in the dendrite tip is much higher than that in the center of dendrite.

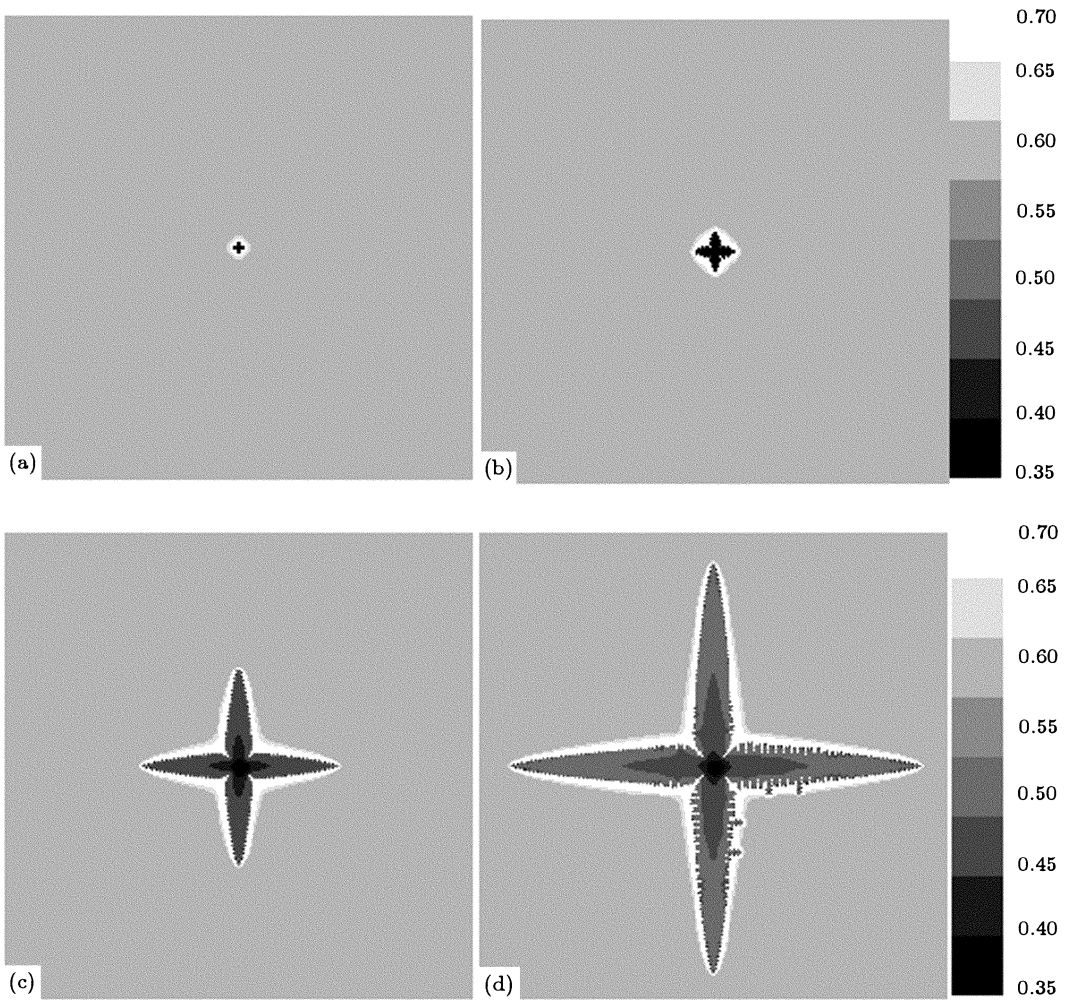


Fig.7. Dendrite morphology as Gibbs-Thomson coefficient is one tenth of the normal value, t=0.002s, 0.008s, 0.012s and 0.016s respectively.

Figure 8 shows the dendrite morphology at different solidification time while Gibbs–Thomson coefficient is ten times of the normal value. Compared with Fig.1 and Fig.8, it can be found that, as the Gibbs–Thomson coefficient is ten times of the normal value, the dendrite morphology is not easy to lost stability, especially in Fig.8(d). In Fig.8 it can be found that the Gibbs–Thomson coefficient plays an important role in keeping the solid/liquid interface stable. If Gibbs–Thomson coefficient increases, the morphology of dendrite will become more stable. On the contrary, if the Gibbs–Thomson coefficient decreases, the solid/liquid interface will become unstable. In addition, the solute distribution in the dendrite is similar to that in Fig.7.

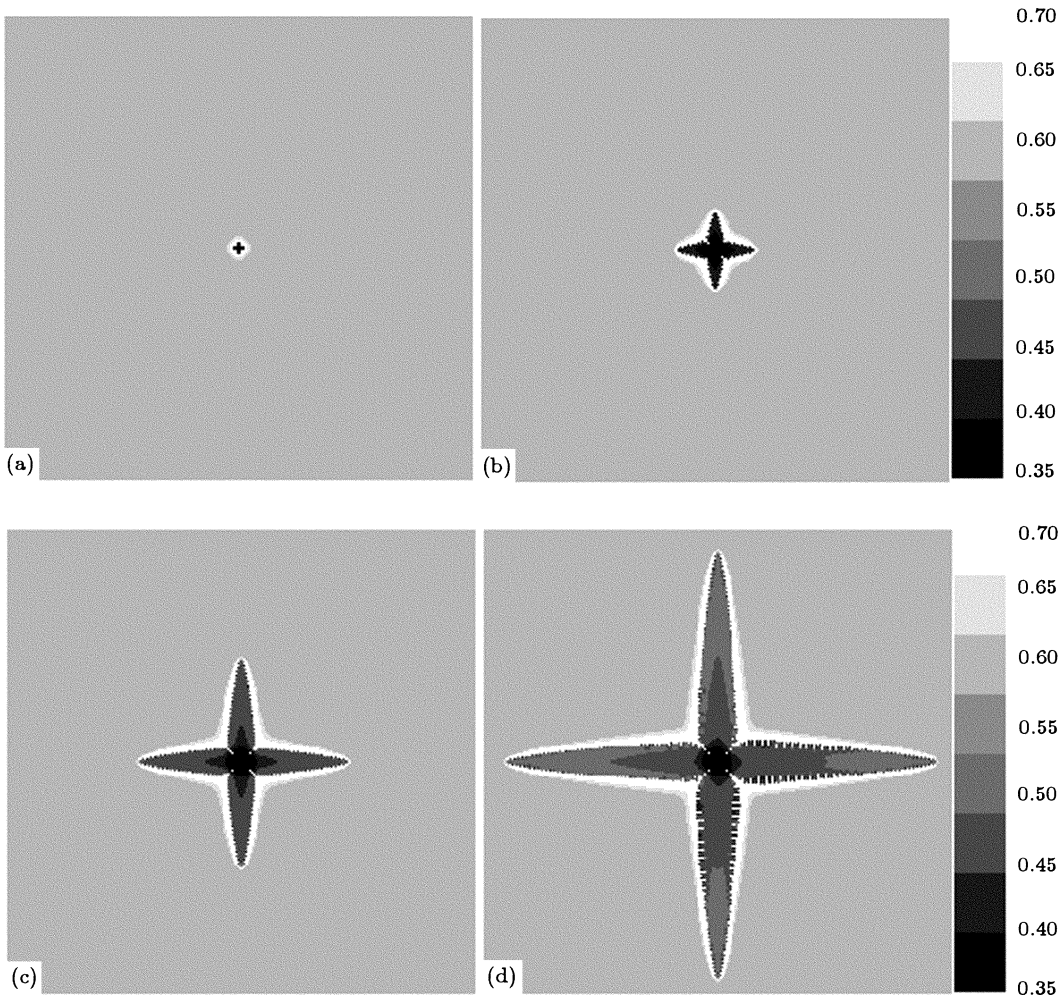


Fig.8. Dendrite morphology as Gibbs–Thomson coefficient is 10 times of the normal value, t=0.004s, 0.008s, 0.012s and 0.016s respectively.

Figure 9 shows that when the liquid solute diffusion coefficient decreases to a half of the normal value, the diameter of the primary dendrite arms is much thinner than the normal one. On the other hand, the solute concentration in the primary dendrite arm is higher than that of the normal value. The reason which causes this phenomenon is that the solute diffusion distance will become shorter as the solute diffusion coefficient decreases. As we know that the solute characteristic length can be expressed as $l_c = D/V$, when V is the interface velocity, l_c is solute characteristic length, hence if D decreases, l_c will decrease too. If the solute ahead of the solid/liquid interface can't diffuse to a more far away place then the new solidified part will contain much higher solute concentration. When the solidification time is 0.016s, in Fig.9(d), the solute concentration near the primary dendrite arm tip is near 0.6%, which is much higher than that in Fig.1(d).

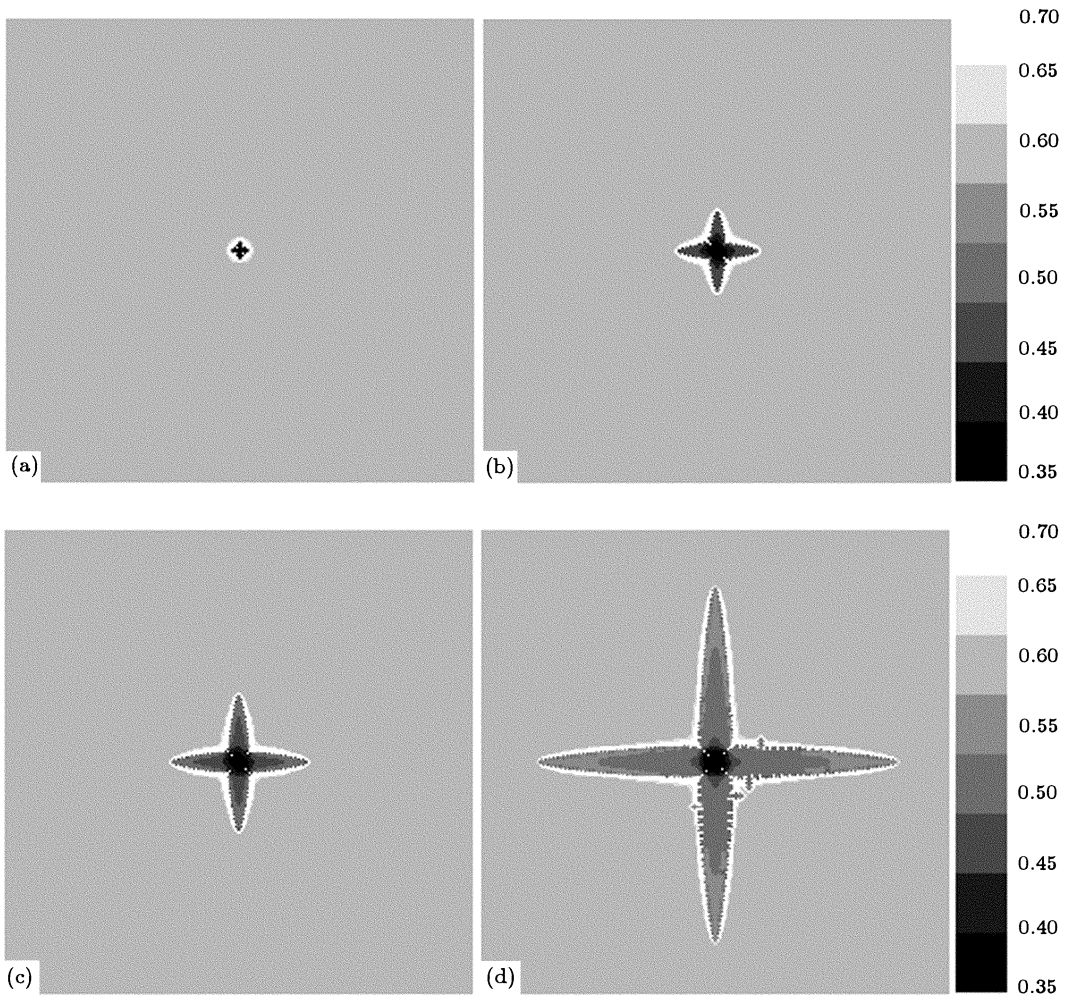


Fig.9. Dendrite morphology at different solidification time when the liquid solute diffusion coefficient is only one half of the normal value, t=0.004, 0.008, 0.012 and 0.016s respectively.

Figure 10 is the dendrite morphology at different solidification time, in which the grey-scale bar in the right side of figure indicates the different solute concentration. Compared the Fig.10 with Fig.9, it is easily found that the dendrite growth velocity of Fig.10 is faster than that in Fig.9, as shown in Fig.9(d) and Fig.10(d). In addition, the solute concentration difference in the primary dendrite arms is smaller than that in Fig.1. Furthermore, Fig.10 shows that when the solidification time is 0.016s the second dendrite arms rise more easily in Fig.10 than that in Fig.1, especially in Fig.10(d). Moreover, Fig.10 indicates that the solute concentration in the primary dendrite arm in Fig.10 is much lower than that in Fig.1 because the liquid solute diffusion coefficient is twice the normal value so that the solute can diffuse more easily and diffuse more far away place. Finally, the secondary arms easily rise up more easily at the solidification time 0.016s than that in Fig.9. From Fig.9 and Fig.10, the liquid solute diffusion coefficient has a direct impact on the solute distribution, which affects the solute segregation distribution.

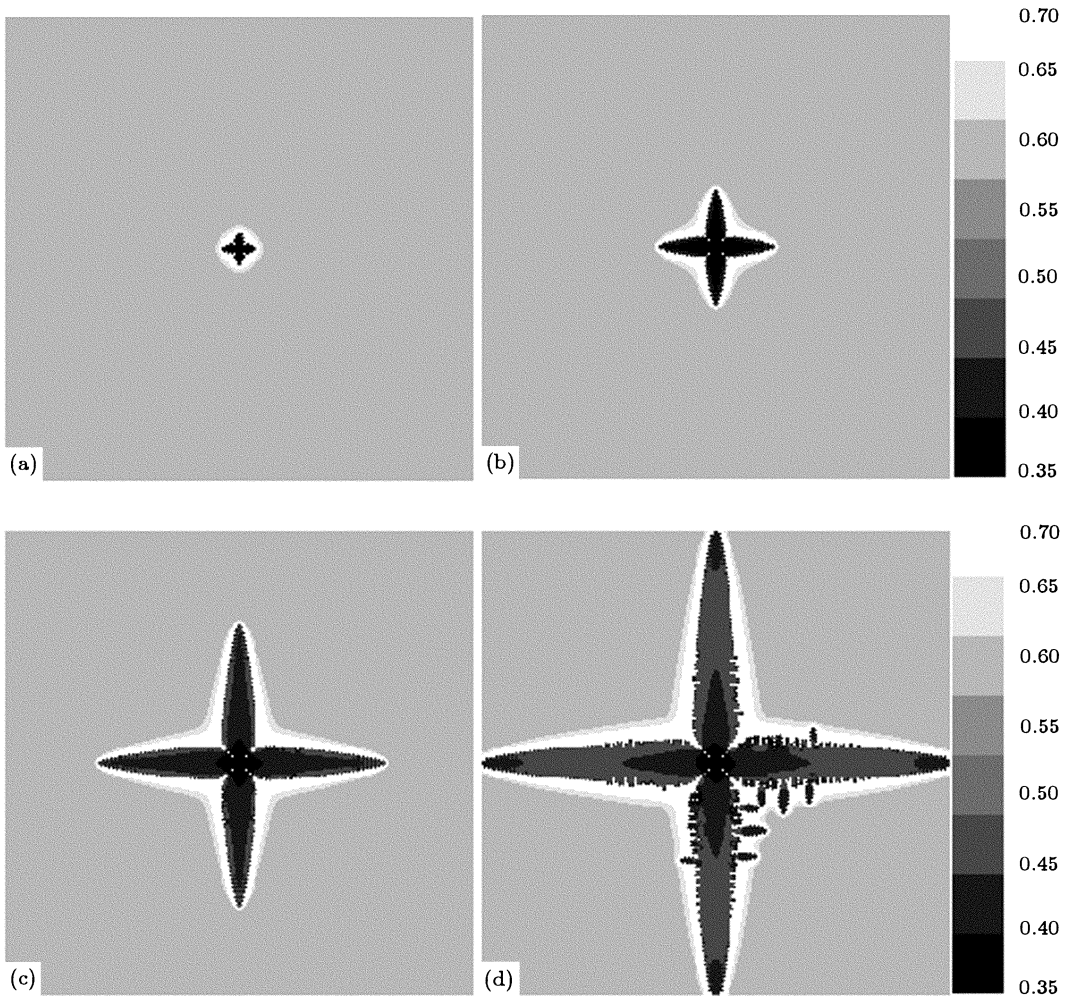


Fig.10. Dendrite morphology at different solidification time as the liquid solute diffusion coefficient is twice the normal value, t=0.004, 0.008, 0.012 and 0.016s respectively.

4. Conclusion

A new model is presented to simulated dendrite evolution and solute segregation in this paper, and then a solidification microstructure is simulated by this method. Finally, different Gibbs–Thomson coefficients and solute diffusion coefficients are selected to simulate their influences on the dendrite morphology. The following conclusion can be drawn according to the above simulating results:

1. this method can simulate the dendrite evolution and microsegregation during solidification process, instead of assuming the interface shape and position to calculate the solid fraction of the solid/liquid interface unit;

2. the advancing dendrite tip is consisted with parabolic growth, which reflects that the model is reasonable;

3. during dendrite solidification process, the highest temperature is in the middle of centreline, and as the solidification time increases, the temperature differences among the dendrite arms increase;

4. when two dendrites meet, there will be a rich solute concentration zone between the two dendrites;

5. when the Gibbs–Thomson coefficient increases, the solid/liquid interface become stable, on the contrary, when the Gibbs–Thomson coefficient decreases, the solid/liquid interface is easier to be unstable;

6. when the liquid solute concentration increases, the solute segregation in the dendrite decreases, on the contrary, the solute segregation in the dendrite will increase;

7. the model can be extended to multicomponent alloy solidification, and this work is undertaking now.

References

[1] Amar B and Brener E A 1993 *Phys. Rev. Lett.* **71** 589

[2] Brener E A 1993 *Phys. Rev. Lett.* **71** 3653

[3] Brener E A 1996 *J. Cryst. Growth* **166** 339

[4] McFadden G B, Coriell S R and Sekerka R F 2000 *J. Cryst. Growth* **208** 726

[5] Spittle J A and Brown S G R 1989 *Acta Metal.* **37** 1803

[6] Gandin Ch A and Rappaz M 1993 *Acta Metal. Mater.* **41** 345

[7] Karma A and Rappel W J 1999 *Phys. Rev.* E **60** 3614

[8] Juric D and Tryggvason G 1996 *J. Comput. Phys.* **123** 127

[9] Kim Y T, Goldenfeld N and Dantzig J 2000 *Phys. Rev.* E **62** 2471

[10] Li M E, Yang G C and Zhou Y H 2005 *Acta Phys. Sin.* **54** 454 (in Chinese)

[11] Li M E, Yang G C and Zhou Y H 2005 *Chin. Phys.* **14** 838

[12] Dilthey U, Pavlik V and Reichel T 1997 *Mathematical Modeling of Welding Phenomena, Conference* Cerjak H and Bhadesia H K D H (Eds.) (The Institute of Materials, The University of Cambridge, UK) p85

[13] Sasikumar R and Sreenivisan R 1994 *Acta Mater.* **42** 2381

[14] Zhu M F, Kim J M and Hong C P 2001 *ISIJ Int.* **41** 992

[15] Nastac L 1999 *Acta Mater.* **47** 4253

[16] Jacot A and Rappaz M 2002 *Acta Mater.* **50** 1909

[17] Sanchez L B and Stefanescu D M 2003 *Metal. Mater. Trans.* A **34** 367

[18] Li Q, Li D Z and Qian B N 2004 *Int. J. Cast. Metal. Res.* **17** 339

[19] Li Q, Li D Z and Qian B N 2004 *Acta Phys. Sin.* **53** 3477 (in Chinese)